ELSEVIER

Solid State Ionics 126 (1999) 3–24

SOLID STATE IONICS

www.elsevier.com/locate/ssi

Studies of the layered manganese bronzes, $Na_{2/3}[Mn_{1-x}M_x]O_2$ with M = Co, Ni, Li, and $Li_{2/3}[Mn_{1-x}M_x]O_2$ prepared by ion-exchange

J.M. Paulsen[a], J.R. Dahn[b,*]

[a] *Department of Physics, Dalhousie University, Halifax, Nova Scotia, Canada B3H 3J5*
[b] *Departments of Physics and Chemistry, Dalhousie University, Halifax, Nova Scotia, Canada B3H 3J5*

Received 7 May 1999; accepted 24 May 1999

Abstract

Layered sodium manganese bronzes, $Na_{2/3}MO_2$ ($M = Mn_{1-x}A_x$, A = Co, Li, Ni) with the P2-structure were investigated. A phase diagram (composition–structure–temperature diagram) for materials synthesized in air is presented. Substitution extends the stability region of P2 phases toward lower temperatures. $Na_{2/3}MnO_2$ exhibits a monoclinic distortion. Weakly substituted samples exhibit an orthorhombic distortion of the ideal P2-structure whereas heavily substituted bronzes adopt the ideal P2-structure. Dry samples exhibit larger distortions than samples exposed to air. The layered sodium bronzes were used to prepare layered Li-transition metal oxides by ion-exchange. Layered Li–Mn oxides with O2-structures were prepared from these bronzes for the first time. As an example crystalline $Li_{2/3}[Ni_{1/3}Mn_{2/3}]O_2$ with the O2 structure was prepared.

Keywords: Sodium manganese bronzes; Phase diagram; Rietveld refinement; Ion-exchange reaction and layered structures

1. Introduction

Layered phases have interesting chemical and physical properties. They often allow the reversible insertion and extraction of cations or protons so they can be used as electrodes in rechargeable batteries. Layered $LiCoO_2$ or $LiNiO_2$ are important cathode materials for Li-ion batteries. Recently, renewed attention has been paid to layered sodium manganese bronzes. This is because sodium manganese oxides can be used as the starting material for ion exchange reactions [1]. This soft chemical route is often the only way to prepare meta-stable layered phases. Examples are the preparation of meta-stable layered lithium manganese oxide $LiMnO_2$ [2,3] (which has the O3 structure) or of $LiCoO_2$ [4] (with the O2-structure) by ion exchanging the corresponding sodium transition metal bronze, Na_xMO_2.

Sodium manganese bronzes are stable in many different structures. In 1971 Parant et al., suggested a phase diagram for Na_xMnO_2 [5]. Depending on temperature and composition, Na_xMnO_2 occurs in different layered phases (α-$NaMnO_2$, α- and β-$Na_{0.7}MnO_2$), as channel structures ($Na_{0.44}MnO_2$) and in other structures.

Though layered transition metal oxide bronzes may crystallize in several different structures, a helpful systematization is possible, see for example [6]. This approach is based on different possible

*Corresponding author.

0167-2738/99/$ – see front matter
PII: S0167-2738(99)00147-2

types of hexagonal stacking of the oxygen sublattice. The transition metal is bound in octahedral sites between two layers of oxygen yielding rigid MO_2 sheets. Here in the notation of stacked hexagonal layers, large letters are used for the oxygen positions and small letters for the transition metal cation positions. Small Greek letters give the alkali metal position. A MO_2 sheet with octahedral cation coordination is written as AbC (or cyclic permutations) or CbA.

The larger alkali cation (Li^+or Na^+) is sandwiched between the MO_2 sheets. Lithium prefers octahedral sites whereas sodium accepts octahedral or trigonal prismatic sites. According to Ref. [6] four structural types are commonly found: P2, P3, O2 and O3[1]. They are distinguished by the type of alkali cation site (P for prismatic and O for octahedral) and by the number of MO_2 sheets in the unit cell.

Layered $LiMO_2$ normally adopts the O3 structure (AbC α BcA β CaB γ . . .). The O2 structure (AbC α BaC β . . .) is metastable. Na_xMnO_2 adopts either O3, P2 or P3. The P2 structure is (AbC * CbA ‘ . . .) where the asterisk (and the apostrophe) mark sodium in one of two possible prismatic sites (α or β for the asterisk, γ or β for the apostrophe). The P3 structure is AbC * CaB ‘‘ BcA ‘ . . .). P2 and O2 are related to each other by a gliding of the MO_2 sheets, which is possible in ion exchange reactions at room temperature. The same is true for O3 and P3. Therefore, by ion exchanging Na with Li, layered Li_xMO_2 with an O2 structure can be prepared from the corresponding P2–Na_xMO_2 bronze. Li_xMO_2 with the O3 structure can be prepared from the corresponding P3 or O3 Na_xMO_2. However, a transformation of O2 or P2 to O3 or P3 is not possible by gliding since it involves breaking Mn–O bonds.

Here, we study doped sodium manganese bronzes based on $Na_{0.7}MnO_2$ that we assume is better written as $Na_{2/3}MnO_2$. We are mainly interested in P2 phases. Beside its potential application as cathodes in Na-ion batteries [7–9] they could allow the preparation of new layered lithium manganese oxides. These materials are of interest as cathodes for lithium batteries since they do not convert to spinel during cycling [10].

Li, Co, and Ni were chosen as dopants. They all can replace manganese on octahedral sites leading to equilibrium phases $Na_{2/3}[Mn_{1-x}M_x]O_2$ (M = Li, Co, Ni). In air they crystallize as P2 or P3 phases or are phase mixtures, depending on temperature and doping. To investigate the phase diagram as a function of doping and temperature, X-ray diffraction, Rietveld refinement, and TGA were used.

The average manganese oxidation state in equilibrium with the gas phase, say air, changes with the temperature. MnO_2 (with tetravalent Mn) is stable until ≅415°C. Between 415°C and ≅910°C Mn_2O_3 (trivalent) is stable. Above ≅910°C Mn_3O_4 (average oxidation state = 2.67) is stable [11]. The same general trend is observed for Na_xMnO_{2+y}. However, the alkali cations within the structure apparently stabilize a higher oxidation state of manganese compared to the pure oxide. β-$Na_{0.7}MnO_{2.05}$ has a Mn oxidation state of 3.4 but it is a high temperature phase. According to Parant et al. [5] it is stable up to 1000°C. At much lower temperatures a similar but oxygen rich phase α-$Na_{0.7}MnO_{2.25}$ with increased Mn oxidation state (3.8) is stable [5].

What occurs if a partial substitution for Mn is made? If Mn is replaced by a cation with lower oxidation state, i.e. Li, then $Na_{2/3}[Mn_{1-x}Li_x]O_2$ has a higher Mn oxidation state than that of the unsubstituted $Na_{2/3}MnO_2$. Consequently, the stability region of the doped phase is expected to move to lower temperatures. The same can be expected for Co and Ni doping since both dopants prefer the lower oxidation states than Mn (3 for Co and 2 for Ni). We show that substitution allows the P2 sodium manganese oxide phases to be stabilized at lower temperatures.

In this work ‘‘equilibrium chemistry’’ was used to prepare the thermodynamically stable manganese bronzes. Equilibrium chemistry means that the temperature was high enough and that the reaction proceeds for a sufficient time to ensure a final state very near thermal equilibrium. Metastable phases such as layered Li–Mn oxides were prepared by soft chemical routes such as ion exchange reactions. Here the temperatures must be low enough to suppress phase transformations to equilibrium phases.

[1]In principle, O1 could be possible but unlike layered sulfides, O1 is the exception for oxides.

2. Experimental

2.1. Preparation of the thermodynamically stable $Na_{2/3}Mn_{1-x}M_xO_2$

Equilibrium phases of $Na_y[Mn_{1-x}M_y]O_z$ (M = Co, Ni, Li) bronzes were prepared by solid state reaction from stoichiometric amounts of Na_2CO_3, Co_3O_4 (Aldrich), EMD (electrolytic manganese dioxide) (Chemetals), NiO (Inco), $Ni(OH)_2$ (Aldrich) or Li_2CO_3 (FMC). The powders were milled together, then pellets were pressed. The pellets were heated in air and then the pellets were quenched in liquid nitrogen and ground to powder. New pellets were pressed and the procedure was repeated. Typical reaction times were 12 h at 1000°C, 16 h at 900°C, 24 h at 800°C, 2 days at 700°C and 4 days at 500°C.

In special cases a thermal treatment of the prepared bronzes was made. Two methods, ''soft oxidation'' or ''thermal shock'' were used. Soft oxidation was made by cooling a sample from the high preparation temperature to an intermediary temperature (e.g. 500°C) followed by tempering it typically for 30 min. Thermal shock was made in the following way: 2 g of powder was put into a large platinum crucible that had been preheated to the reaction temperature. A typical temperature to perform thermal shock is 1000°C. The hot crucible was put into the hot furnace and a reaction was performed for a short time (e.g. 8 min). Then the powder was quenched by pouring into liquid nitrogen.

Some of the powders produced are slightly hygroscopic. Two kinds of X-ray investigations were made. One is to allow a water uptake of the powder by exposing it to air for some time ($\approx$1day) before the X-ray investigation. The other is to exclude any water uptake: Directly after the quenching of the pellets they were heated in vacuum for 1 h at 200°C. From the furnace they were directly imported to a helium-filled glove-box and ground. The X-ray investigation was performed using a gas tight sample holder filled with helium. The X-ray beam penetrated into and out of this holder through an aluminized mylar window.

X-ray data were collected using a Siemens D500 diffractometer using copper K_α-radiation. Powders of layered materials can show preferred orientation in diffraction patterns. To diminish this effect, the powder was sieved onto a zero-background holder wetted with acetone. The holder is a single crystal Si wafer, cut in the 510 direction. The profile refinement of the collected data was made using Hill and Howard's version of the Rietveld program [12,13].

In the Rietveld refinements the occupation of oxygen and the alkali (sodium or lithium) sites were freely varied. The occupation for the transition metal was fixed to $n = 1$. One global isotropic temperature factor is refined. A relaxation of the spectrum due to preferred orientation was allowed. The obtained atomic occupation numbers for oxygen are rather reliable compared with those of lithium and sodium which have larger error bars. This is caused by a competition between alkali atom occupation number and preferred orientation as well as by the weak scattering power of Li and the large in-plane motion of sodium.

2.2. Preparation of metastable Li_xMO_2 by exchange reactions

Sodium in Na_xMO_2 was ion exchanged by lithium. Typically 5 g of Na_xMO_2 was stirred for 2–5 h in a solution of LiBr (55 g) in hexanol (150 ml) while refluxing. This corresponds approximately to a 10 times excess of lithium in a 5 M solution. The reaction temperature was the boiling point of the solution i.e. $\approx$180°C. After reaction the solution was filtered under suction, and the remaining powder was washed in methyl alcohol. Usually, the LiBr and Na_xMO_2 as well as the reaction product were dried in vacuum for 2 h at 200–250°C.

Alternatively ion exchange in molten salt was attempted. The molten salt used was 14 g of a eutectic mixture of 88 mol% $LiNO_3$ and 12 mol% LiCl [14]. Typically 2 g of Na_xMO_2 (this corresponds to $\approx$10 times Li excess) was put into the melt and the reaction was performed for 1 h at 280°C. After reaction the mixture was washed either in ethanol or water, filtered and then the reaction product was dried at 200–230°C in vacuum for 2 h.

2.3. Thermogravimetric analysis (TGA)

A TA instruments 910 thermal gravimetric analyzer was used. Typically 40 mg of powder were placed in a platinum boat. The measurement was

made in a flow (≈ 5 l/h) of extra dry air (No CO_2 or water, Linde). Typical temperature sweep rates were 2 K/min. The data were corrected for the change in the buoyant force of air with temperature. The data necessary for the correction were obtained by performing a TGA experiment on 30 mg of inert Al_2O_3 powder.

3. Results

3.1. Overview

The first section deals mostly with Na_xCoO_2 and its ion-exchanged derivatives $LiCoO_2$. Cobalt bronzes are easy to prepare and ion exchange works very well. The crystal structures are easily understood since they are not distorted. (Unlike manganese, cobalt does not tend to Jahn–Teller-distort the lattice or cation mix with lithium). The intention of this section is merely to display general and typical properties, explain the structures, which can be expected, and to compare the results with results from literature.

The second section deals with undoped Na_xMnO_z and its derivative Li_xMnO_2. The third section deals with the substituted $Na_x[Mn_{1-y}M_y]O_z$ bronzes. Dopants are Co, Li and Ni. It will be shown that doping extends the stability region of the desired P2 structures. Composition–structure–temperature diagrams are given. The structure of the derived Li_xMO_2 phases is analyzed. An additional section deals with the thermal and chemical stability of the bronze phases.

3.2. Cobalt bronzes Na_xCoO_2 and their derivatives Li_yCoO_2

3.2.1. P2–$Na_{2/3}CoO_2$

In oxygen, Na_xCoO_{2+z} adopts the desired P2 structure above $\cong 650$°C for $0.6 \leq x \leq 0.75$ [15]. At lower temperatures $Na_{0.6}CoO_2$ adopts the P3 structure for $0.55 \leq x \leq 0.6$ and O3 structures are stable for $1 \leq x \leq 0.9$ and $x = 0.75$ [15].

We synthesized P2–$Na_{2/3}CoO_2$ in air at 700, 800, 900 and 1000°C. A typical X-ray pattern ($Na_{2/3}CoO_2$ at 900°C) together with a calculated pattern obtained by a Rietveld refinement and the corresponding crystal structure is given in Fig. 1. The lattice parameters (atomic positions, atomic occupation numbers and lattice constants) are displayed as well in the plot. The crystal structure is the ideal P2 structure, space group P63/mmc (number 194).

The sample prepared at 1000°C differs from all others. It lost more weight and was densely sintered. The X-ray spectrum could still be indexed as P2, however the intensities changed significantly. Perhaps significant sodium evaporation and oxygen release occurred. To correlate this result with the thermal stability of $Na_{2/3}CoO_2$, a TGA measurement was made (Fig. 2). The results confirm that $Na_{2/3-y}CoO_{2-z}$ prepared at 1000°C is oxygen ($z > 0$) and sodium deficient ($y > 0$) which will be explained in the following.

The mass versus temperature during heating shows four regions: a slight increase of mass up to ≈ 400°C followed by a mass loss of $\approx 1.5\%$ up to ≈ 600°C (region 1); between 600 and 800°C the mass stays constant (region 2); between 800 and 950°C another $\approx 2\%$ mass loss is observed (region 3) and finally a large amount ($\approx 4\%$) is suddenly lost above 960°C (region 4). It is important that this mass loss does not continue while the sample is held isothermally at elevated temperature. During cooling, more than half of the mass lost during region 3 and 4 is regained. After the measurement the sample was tightly sintered to the platinum boat.

The results can be interpreted as follows: The first part of region 1 (until 400°C) is the superposition of the mass loss of adsorbents and a mass gain by a reaction of P2–$Na_{2/3}CoO_2$ to oxygen rich (and probably meta-stable) P2–$Na_{2/3}CoO_{2+z}$. A similar reaction occurs for P2–$Na_{2/3}MnO_2$ that will be discussed later. The mass loss at the end of region 1 is the oxygen release to yield the stable P2–$Na_{2/3}CoO_2$ which remains during region 2. The irreversible mass loss during region 3 could be a loss of oxygen or an evaporation of sodium. However, the abrupt mass loss during region 4 must be a release of oxygen from $Na_{2/3}CoO_2$ in equilibrium with the gas flow. It cannot be sodium evaporation since this would not be reversible and especially would not stop immediately after the final temperature is reached. This oxygen release could either be

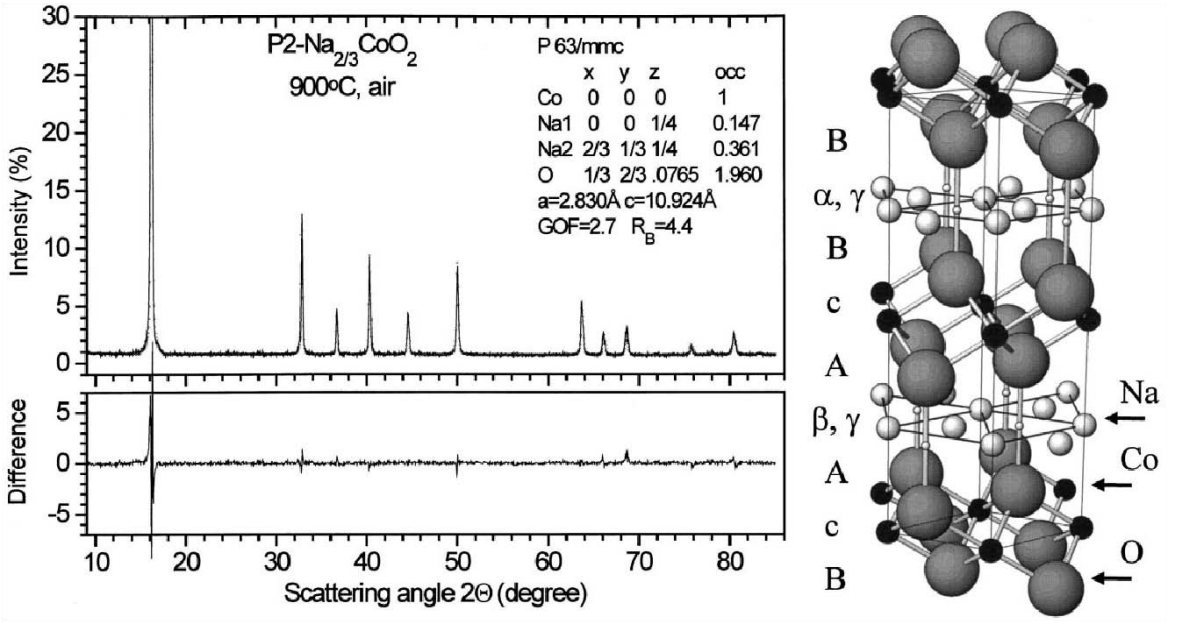

Fig. 1. X-ray diffraction results, Rietveld refinement and crystal structure of P2–$Na_{2/3}CoO_2$. The oxygen stacking is ABBA. Co is located in octahedral sites and Na in prismatic sites. The P2 structure allows two different Na positions that are each partly filled. The sites displayed by small spheres are empty.

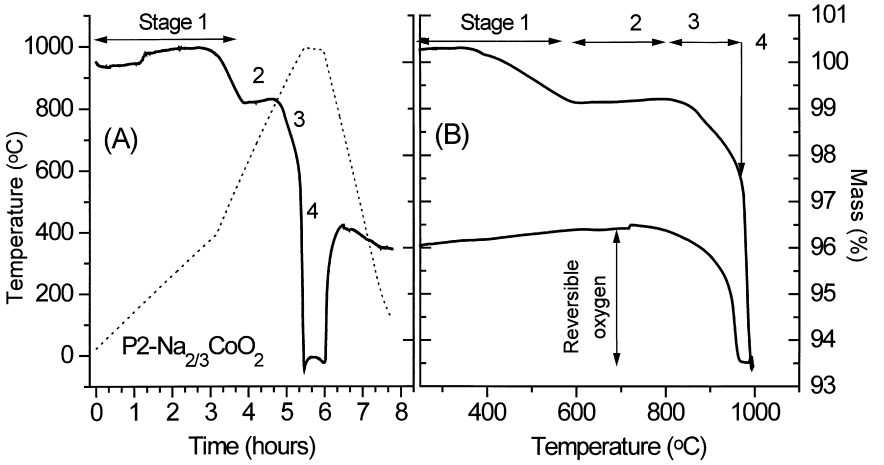

Fig. 2. TGA of P2–$Na_{2/3}CoO_2$ in extra-dry (no CO_2 or water) air. The left and right plot display the same set of data using a different *x*-axis.

$Na_{2/3}CoO_2$ in equilibrium with the gas phase ($Na_{2/3}CoO_2 \Leftrightarrow Na_{2/3}CoO_{2-\varepsilon} + \varepsilon/2O_2$) or the reversible decomposition of $Na_{2/3}CoO_2$ to something and CoO, such as $1.5Na_{2/3}CoO_2 \Leftrightarrow NaCoO_2 + 1/2CoO + 1/4O_2$. In the latter case the back reaction must be very fast since the sample prepared at 1000°C (and quenched!) showed an X-ray spectrum of the P2 phase but no cobalt oxide. The first case

indicates a huge oxygen non-stoichiometry range since 3% mass corresponds to $z \cong 0.2$.

3.2.2. O2–$LiCoO_2$

Delmas et al., suggested ion exchanging the sodium in P2-bronzes by lithium [1]. Since lithium does not prefer the prismatic sites, the CoO_2 layers will glide to make octahedral sites. The gliding could occur in different ways leading to O2, O4 or O6 structures, see for example [10].

We prepared O2–$LiCoO_2$ from P2–$Na_{2/3}CoO_2$ by ion exchange of LiBr in hexanol. Delmas et al. [4] suggested that $LiCoO_2$ (caused by the instability of the Co^{4+} cation) instead of the expected $Li_{2/3}CoO_2$, is the reaction product. This is confirmed by our results. After reaction the hexanol is deep green-blue, indicating dissolved Co. We made a TGA experiment on the product powder (Fig. 3). If the composition were $Li_{2/3}CoO_2$, then during the slow heating an irreversible decomposition to the thermodynamically stable O3–$LiCoO_2$ and cobalt oxide would occur: $1.5Li_{2/3}CoO_2 \Rightarrow LiCoO_2 + 1/6Co_3O_4 + 1/6O_2$. At high temperatures the cobalt oxide would decompose $1/3Co_3O_4 \Rightarrow CoO + 1/6O_2$. In a TGA experiment significant mass losses would be visible. This is not the case, proving a stoichiometry near Li_1CoO_2.

If the ion exchange is performed in molten salt $Li_{2/3}CoO_2$ is still not formed. During exchange the salt becomes a foam, indicating that oxygen or nitrogen is released caused by a reaction with the melt. However, the resulting O2–$LiCoO_2$ is less pure.

The ion exchange of the O2–$LiCoO_2$ in hexanol is almost completed. Fig. 4 shows the X-ray diffractogram, the Rietveld refinement and explains the structure. The sample contains impurities indicated by tiny remnants of the initial phase ($Na_{2/3}CoO_2$, marked by an asterisk) and the thermodynamically stable O3–$LiCoO_2$ (marked by arrows). The O2–$LiCoO_2$ was investigated as cathode material for rechargeable Li-batteries. It shows a similar capacity to O3–$LiCoO_2$ and can be charged and discharged with very high rates. These results will be presented in a following publication.

3.2.3. P3- and O3 phases

The previous section displayed that ion exchange of P2 structures yield O2 structures. It would be interesting to show that ion exchange of P3 does yield O3 instead. We were not able to prepare P3–Na_xCoO_2 in air. At 500°C no crystalline layered phase was achieved, and at 600°C P2-type phases evolved. However, doping with manganese stabilized the P3-type phase. Solid state reaction in air at 700°C yielded P3–$Na_{2/3}[Co_{0.7}Mn_{0.3}]O_2$ which could easily be ion-exchanged in hexanol to give a layered O3-type phase. The X-ray diffraction pattern, the Rietveld refinement and the structures are shown in Figs. 5 and 6, respectively. The stoichiometry of this phase is probably $Li_{2/3}[Co_{0.7}Mn_{0.3}]O_2$.

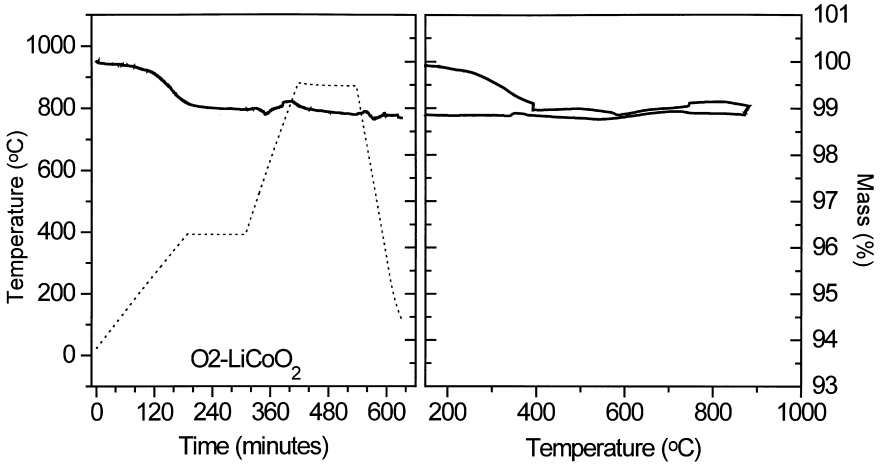

Fig. 3. TGA of O2–$LiCoO_2$ in extra-dry air.

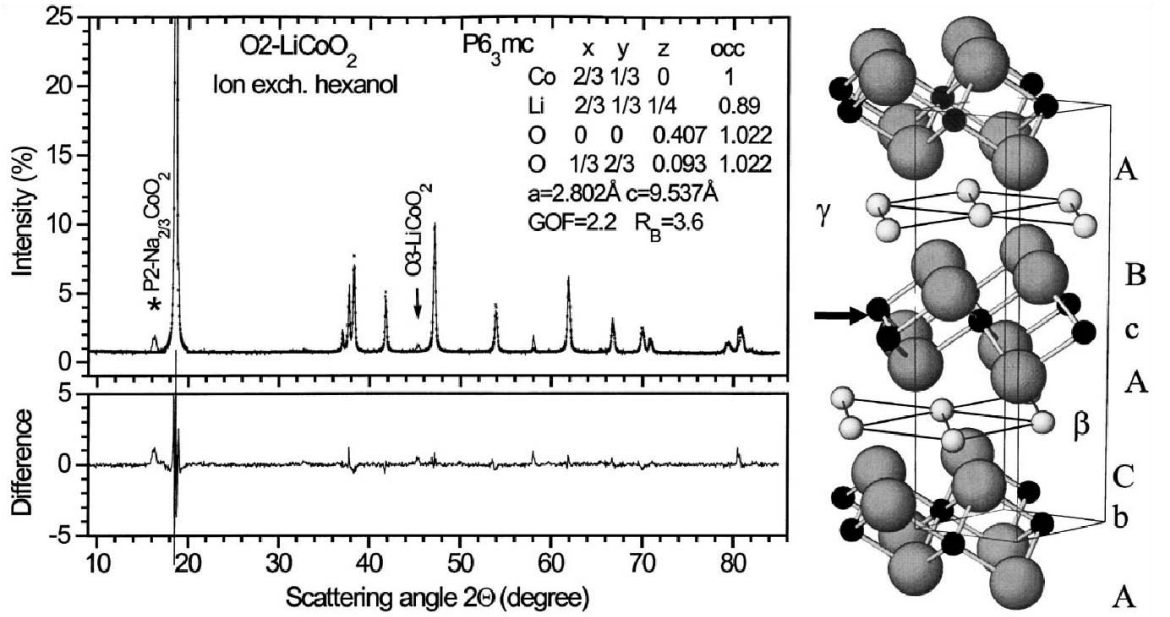

Fig. 4. X-ray diffraction data, Rietveld refinement and crystal structure of O2–$LiCoO_2$. O2 is obtained from P2 by a gliding of the middle CoO_2 layer to the right. Both Mn and Li are located in octahedral sites. The oxygen stacking is ACAB.

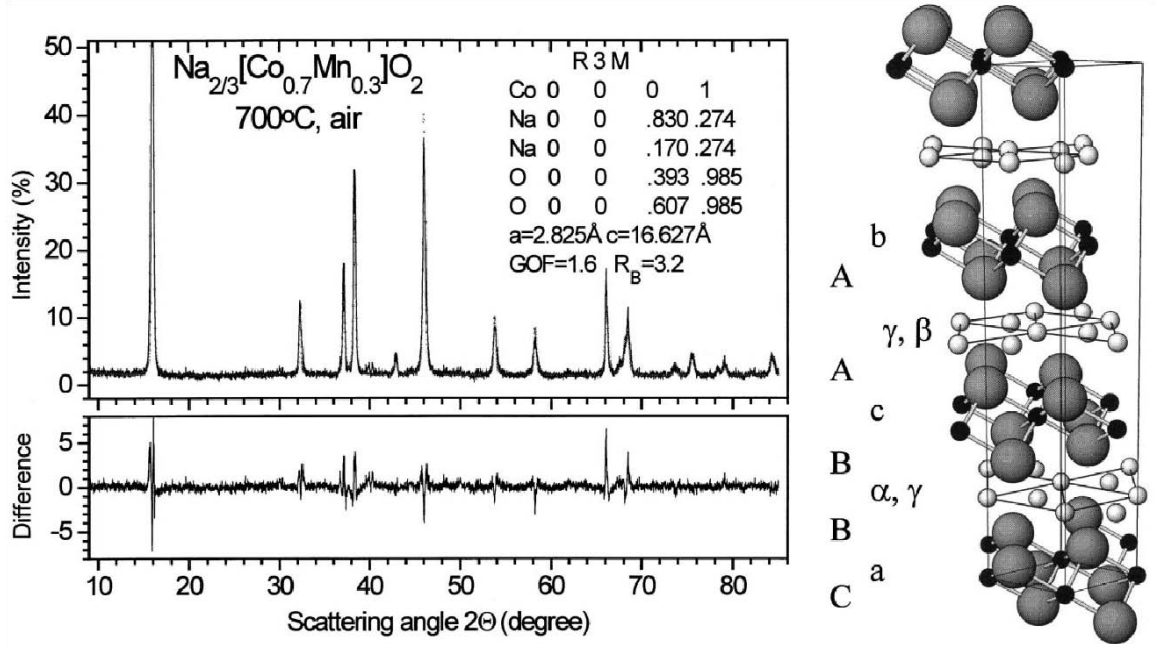

Fig. 5. X-ray diffraction pattern, Rietveld refinement and crystal structure for the ''ideal'' P3-structure. $Na_{2/3}MO_2$ with $M = Co_{0.7}Mn_{0.3}$.

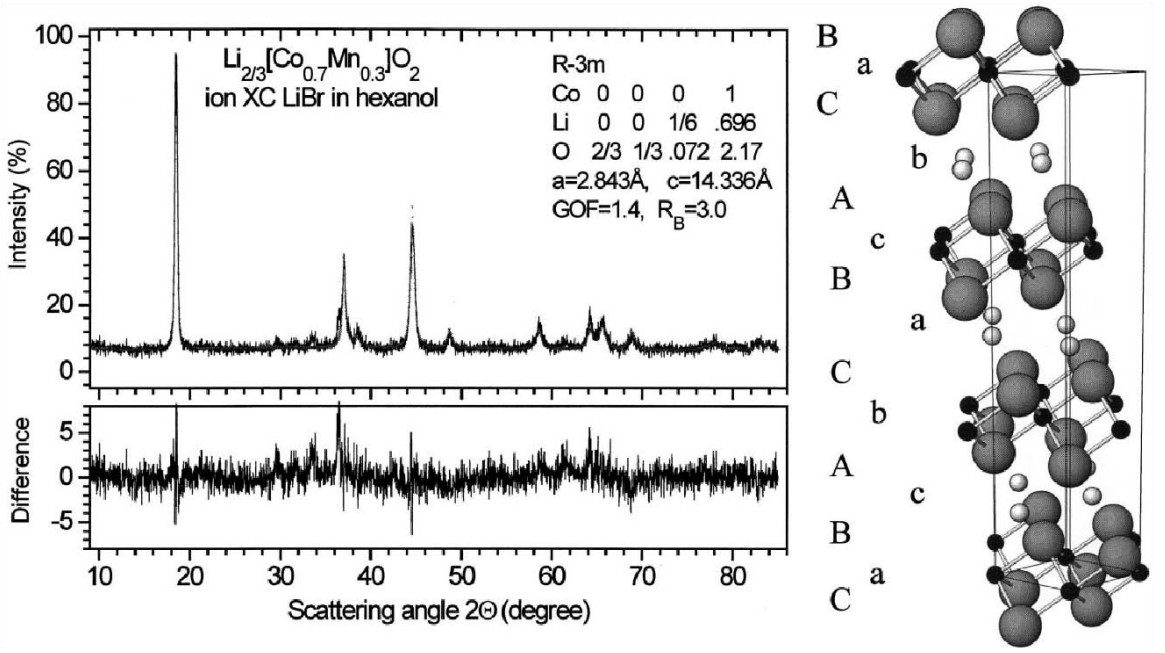

Fig. 6. X-ray diffraction pattern, Rietveld refinement and crystal structure of O3–Li_xMO_2 obtained by ion exchanging P3–$Na_{2/3}MO_2$, $M = Co_{0.7}Mn_{0.3}$.

3.3. Manganese bronzes

3.3.1. $Na_{2/3}MnO_{2+z}$

In 1971 Parant et al. [5] published the phase diagram of Na_xMnO_2 in oxygen. They showed that three different layered phases exist: α-$Na_{0.7}MnO_{2+z}$ ($0.05 \leq z \leq 0.25$) has the ideal P2-structure and is stable below 600°C; β-$Na_{0.7}MnO_{2+y}$ ($y \leq 0.05$) is an orthorhombic distorted P2-structure which is claimed to be stable above 600°C and coexists with α-$NaMnO_2$. α-$NaMnO_2$ is stable between 600 and 850°C and adopts the O3-structure with a monoclinic distortion.

In this work a β-$Na_{0.7}MnO_{2+z}$-type phase (which has a distorted P2-structure) was prepared at 1000°C in air. This phase will be called HT–P2–$Na_{2/3}MnO_2$ (*HT* for *h*igh-*t*emperature). We never achieved single-phase material if the sodium stoichiometry was larger than 2/3 or the temperature below ≅950°C. So we believe that this phase is only stable in air at high temperatures and not at large sodium stoichiometry.

Fig. 7 shows the X-ray diffraction pattern and the Rietveld refinement. The refinement gives a significantly better result if a monoclinic distortion is assumed. However, the monoclinic distortion is small since the monoclinic angle, $\beta = 90.68°$, differs only slightly from $\beta = 90°$.

It was not possible to prepare the undistorted P2–$Na_{2/3}MnO_2$ (corresponding to α-$Na_{0.7}MnO_{2+z}$ in air by solid state reaction below 600°C. At 500°C a single-phase material was obtained which probably is layered. To our best knowledge this phase has not been published previously. In the following we call this phase LT–$Na_{2/3}MnO_2$ (*LT* for *l*ow *t*emperature). The diffractogram is better indexed as P2 than P3. Fig. 8 displays it with the peaks indexed in a hexagonal setting. We were not able to refine the diffraction pattern satisfactorily.

At higher temperatures (≅700°C) in air an undistorted P2–$Na_{2/3}MnO_{2+z}$ is stable. However, X-ray diffraction shows that the crystallinity is poor. A better-crystallized phase with the undistorted P2-structure can be obtained by a special treatment, which we call ''soft oxidation''. The principle of soft oxidation is explained in the following. β-

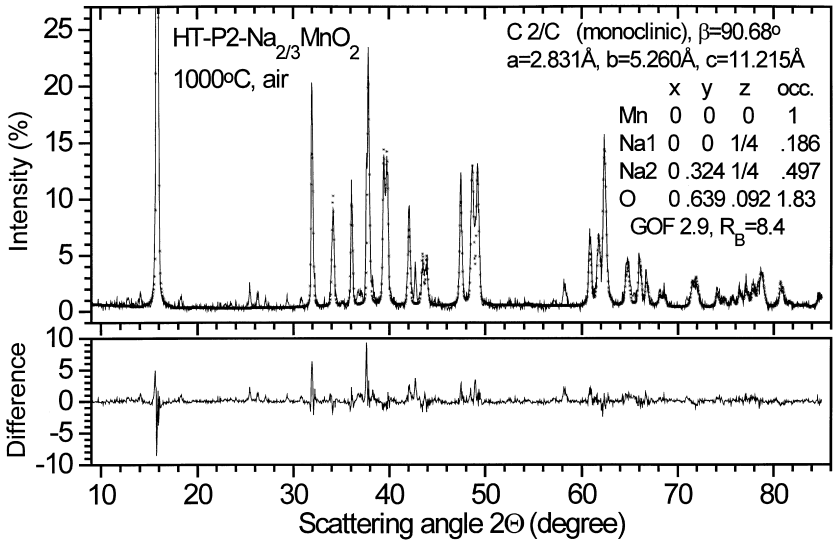

Fig. 7. X-ray diffraction pattern and Rietveld refinement of HT–P2–$Na_{2/3}MnO_2$ prepared at 1000°C. The structure is a monoclinic distorted P2-structure.

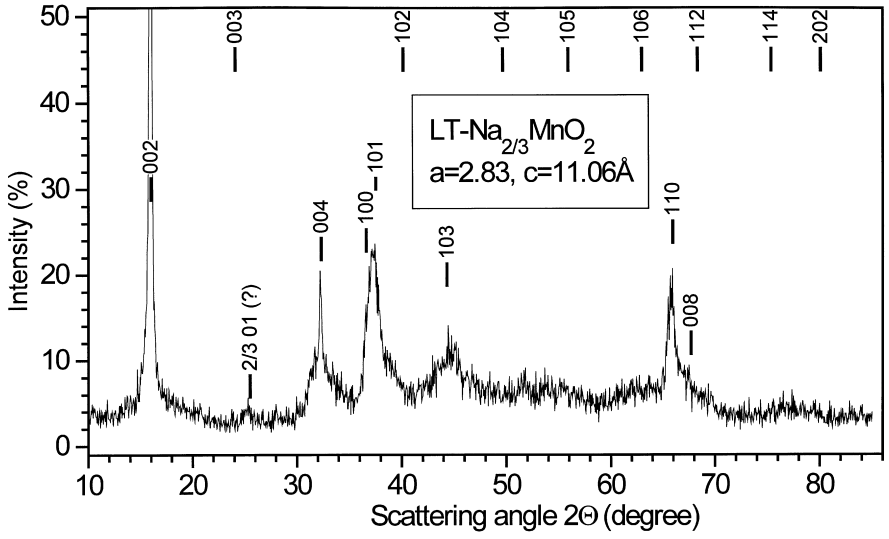

Fig. 8. X-ray diffraction pattern of LT–$Na_{2/3}MnO_2$.

$Na_{0.7}MnO_{2+z}$ ($z \cong 0.05$) has a distorted structure due to the Jahn–Teller effect. This effect is absent for α-$Na_{0.7}MnO_{2+z}$ ($z \cong 0.25$) since the Mn oxidation-state is larger. In addition, we expect that the transformation from P2 to O3 or to P3 will be a slow process since a reordering of the oxygen sub-lattice is required. If β-$Na_{0.7}MnO_{2.05}$ is at elevated temperature and the temperature is lowered then manganese ''wishes'' to increase its mean oxidation state (this is explained in detail in Ref. [16]). Since the phase transformation to the stable low temperature phase (LT–$Na_{2/3}MnO_2$) phase is slow, oxygen is

temporarily added to the P2-structure. By this route from HT–P2–$Na_{2/3}MnO_2$ (which has a structure corresponding to β-$Na_{0.7}MnO_{2+z}$) an undistorted P2–$Na_{2/3}MnO_{2+z}$ (with a crystal structure corresponding to α-$Na_{0.7}MnO_{2+z}$) can be obtained. The X-ray diffraction pattern is given as plot (F) in Fig. 9.

Fig. 10 shows the corresponding TGA measure-

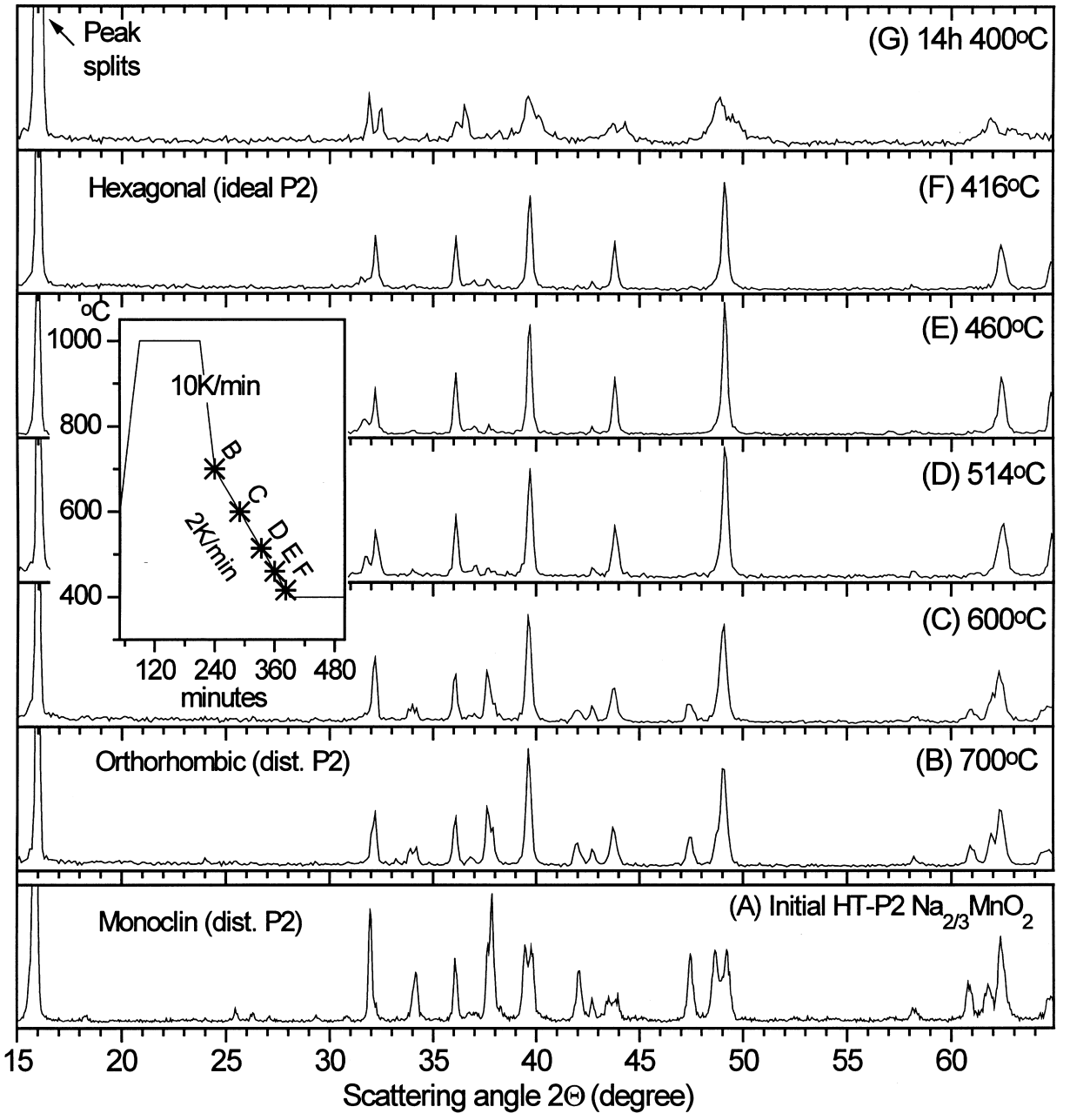

Fig. 9. Series of X-ray diffraction patterns of HT–P2–$Na_{2/3}MnO_2$ during cooling. The initial P2-phase (monoclinic) transforms to the meta-stable phase (from 514 to 416°C) with the ideal P2-structure which then slowly decomposes. The small inset shows the cooling regime.

ment of the transformation of $Na_{2/3}MnO_2$. The mass gain which suddenly occurs during cooling below ≈ 600°C is the oxygen uptake, i.e. the oxidation of HT–P2–$Na_{2/3}MnO_2$ to the undistorted $Na_{2/3}MnO_{2+z}$. The data indicate an oxygen uptake of $z \approx 0.1$ mol. This uptake is reversible, the oxygen is again released above 600°C during re-heating and taken up again during cooling. Fig. 9 shows the structural changes that occur during the cooling. The distortion of the structure of the HT–P2–$Na_{2/3}MnO_2$ first changes from monoclinic to orthorhombic. Significant changes occur below 600°C at the temperature where the oxygen uptake occurs. Some peaks disappear (34.0, 37.8, 42.0, 42.7, 47.5°) and new ones develop (31.8°). At 416°C the $Na_{2/3}MnO_{2+z}$ phase with an undistorted P2-structure evolves. This structure is not stable but meta-stable at this temperature. After heating for 14 h at 400°C, it has decomposed.

3.3.2. Layered Li_xMnO_2 (obtained by ion exchange)

Layered Li_xMnO_2 obtained by ion-exchanging Na_xMnO_2 bronzes are of special interest for application as cathodes in rechargeable batteries. It is known that O3–$NaMnO_2$ can be ion-exchanged to give the layered O3–$LiMnO_2$ [2,3]. O3–$LiMnO_2$ has been investigated as a cathode material for lithium batteries. It has a high initial capacity but this decays significantly in only a few charge-discharge cycles [3]. This is due to the collapse of the O3 structure and a transformation to the more stable spinel-phase during cycling. The collapse is enabled by the fact that the spinel structure and the O3-structure have the same oxygen stacking. O2–Li_xMnO_2 prepared by ion-exchanging P2–Na_xMnO_2 is of great interest because the different oxygen stacking prevents transformation to the spinel phase. Then the O2-phases should show repeated charge-discharge cycling without transformation to spinel [10].

Ion exchange of HT–P2–$Na_{2/3}MnO_2$ was performed using LiBr dissolved in hexanol. The exchange did not complete. The plot (B) of Fig. 11 shows the X-ray diffraction pattern of the obtained phase mixture of HT–P2–$Na_{2/3}MnO_2$ and O2–$Li_{2/3}MnO_2$. From the intensity of the main peak of the initial $Na_{2/3}MnO_2$ phase ($2\Theta = 16°$) about 10% of unreacted phase remains. Neither repeated exchanges nor ion-exchange in molten salt led to any improvement. The diffraction pattern exhibits broad peaks indicating poor crystallinity and stacking faults. Indexing the peaks using the ideal O2-structure is only partly successful. The electrochemical properties of this phase used as a cathode in Li cells are insufficient. In the best case the capacity approaches 100 mAh/g and the rate capability is very poor. It is interesting to compare the poorly crystalline O2–$Li_{2/3}MnO_2$ with the superior O2–

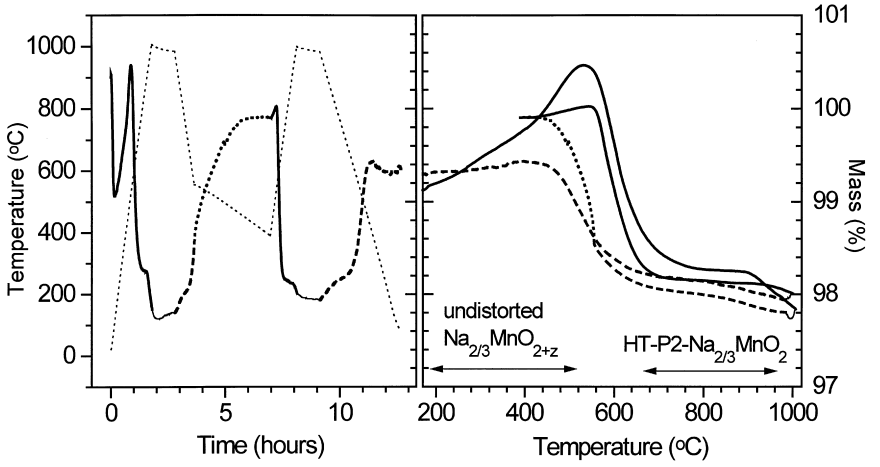

Fig. 10. TGA of P2–$Na_{2/3}MnO_2$. At high temperatures HT–P2–$Na_{2/3}MnO_2$ is stable. The mass gain at low temperatures is due to the formation of the oxygen-rich ideal P2-structure $Na_{2/3}MnO_{2+z}$.

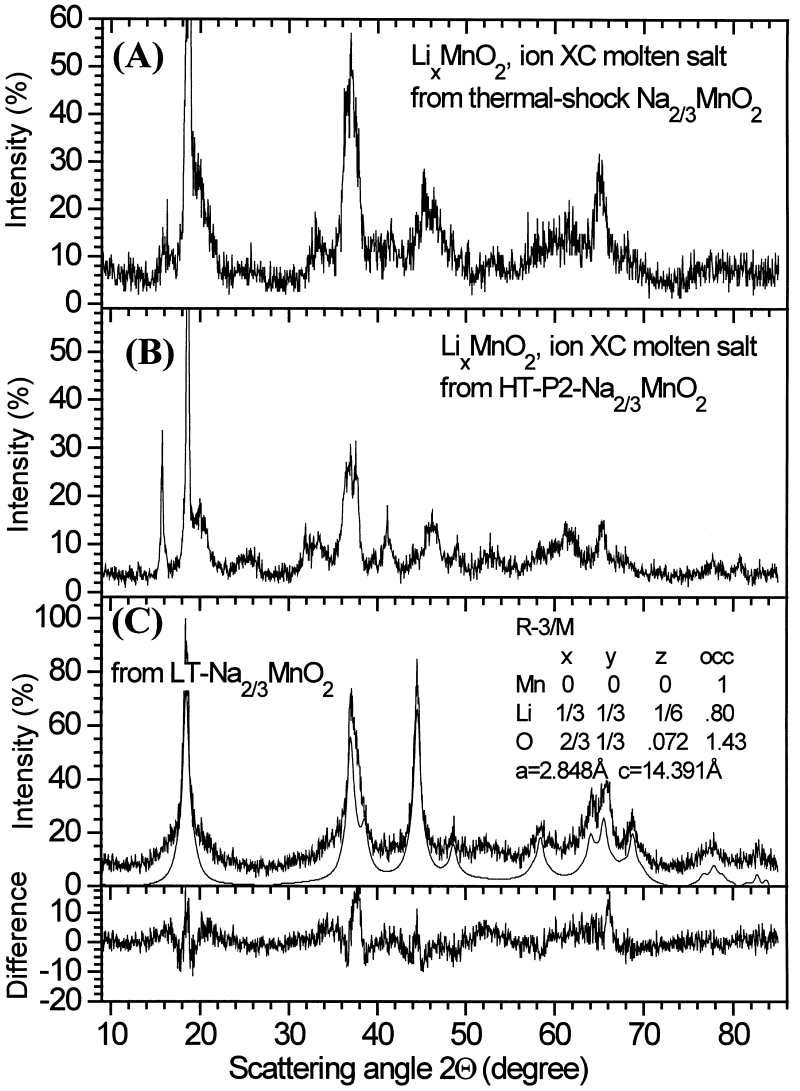

Fig. 11. X-ray diffraction pattern of Li_xMnO_2 prepared by ion exchange from different $Na_{2/3}MnO_2$ phases. (A) Li_xMnO_2 from ''thermal shock''–$Na_{2/3}MnO_2$ (exchange almost complete). (B) Li_xMnO_2 from HT–P2–$Na_{2/3}MnO_2$ (insufficient exchange). (C) Li_xMnO_2 from LT–$Na_{2/3}MnO_2$ (complete exchange) The calculated spectrum is offset for visibility.

$LiCoO_2$. The cobalt material was much more easily ion-exchanged and gave highly crystalline powder compared with the manganese bronze. We believe that this distinction is connected with the ability of $Na_{2/3}CoO_2$ to react to *stoichiometric* $LiCoO_2$ by dissolving the unstable Co^{4+} cation[2].

[2]The corresponding process does not work as well for $Na_{2/3}MnO_2$ since Mn^{4+} is more stable.

Surprisingly, ion-exchange of LT–$Na_{2/3}MnO_2$ easily leads to single phase Li_xMnO_2. The diffraction pattern is shown in plot (C) of Fig. 11. The broad peak tails probably indicate some stacking faults which cannot be simulated by conventional Rietveld analysis. Therefore, we were not able to obtain a satisfactory Rietveld refinement.

O3 α-$NaMnO_2$ and LT–$Na_{2/3}MnO_2$ yielded quite pure Li_xMnO_2 phases whereas the ion-exchange of

HT–P2–$Na_{2/3}MnO_2$ was difficult. The degree of ion-exchange depends not only on composition and crystal structure but is sensitive to preparation conditions. For example, O3 α-$NaMnO_2$, prepared in air at 800°C, did not exchange as well as O3 α-$NaMnO_2$ prepared in argon. The sample made in air was more sintered and had bigger particles. The HT–P2–$Na_{2/3}MnO_2$ was also sintered and difficult to grind. We hoped that an alternative microstructure, with smaller particles typical for lower temperature syntheses, could support the ion-exchange. Therefore we tried to prepare P2–$Na_{2/3}MnO_2$ by a route which we call ''thermal shock''.

LT–$Na_{2/3}MnO_2$ has the preferred small particle microstructure. However, it has a crystal structure that is different from undistorted P2 and it is probably oxygen rich. Microstructure changes, such as sintering, require long range diffusion. This is a slow process compared to oxygen ordering, oxygen release and cation ordering which only require short-range diffusion. Heating a sample to high temperature for a short time (i.e. thermal shock) should lead to material with the typical high temperature crystal structure and composition, but low temperature morphology.

Fig. 12 shows the diffraction pattern of the sample prepared by thermal shock and, for comparison, a pattern of HT–P2–$Na_{2/3}MnO_2$. The peak positions are roughly the same, but there are some differences between the patterns. For the thermal shocked sample, only the peaks at small 2Θ are sharp. Peaks at larger angles are broad. This suggests that the sample consists of small domains of crystalline P2-phase. This phase allowed a nearly complete ion-exchange as shown in plot (A) of Fig. 11. The pattern is typical for O2–Li_xMnO_2 with stacking faults. A similar pattern (for O2–$Li_x[Li_{1/6}Mn_{5/6}]O_2$) will be discussed later.

3.4. P2-Manganese bronzes doped with Co, Li, Ni

3.4.1. Cobalt doping (the solid solution $Na_{2/3}[Mn_{1-x}Co_x]O_2$)

Cobalt doping stabilizes the P2-phases and extends their stability range in temperature. To investigate the phase relations a series of samples with different doping levels ($x = 0$, 15, 30, 50, 70, 100%) was prepared at temperatures between 600 and 1000°C. The left plot in Fig. 13 shows the stability region of the P2 phase. Within the stability region, $Na_{2/3}[Mn_{1-x}Co_x]O_2$ is a single phase. Increasing the Co content moves the lower stability limit towards lower temperatures. At temperatures above the stability region, $Na_{2/3}MO_2$ decomposes by Na

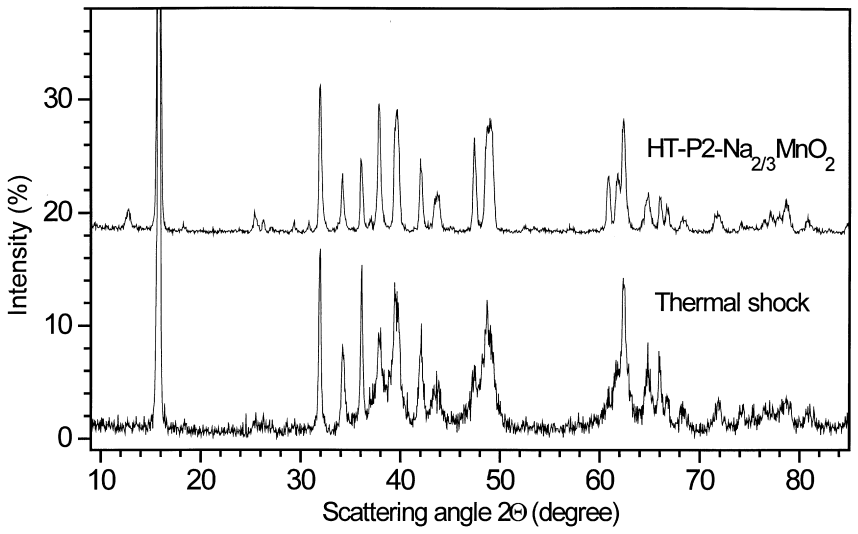

Fig. 12. X-ray diffraction pattern of $Na_{2/3}MnO_2$ prepared by ''thermal shock'' from LT–$Na_{2/3}MnO_2$. For comparison, the pattern for HT–P2–$Na_{2/3}MnO_2$ is also shown.

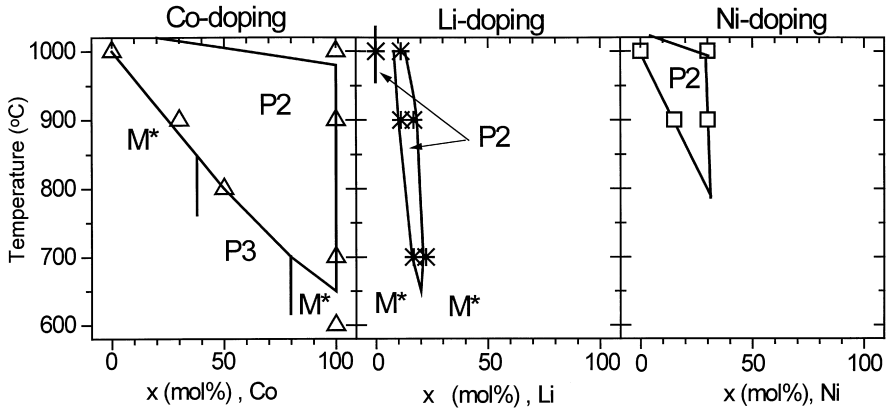

Fig. 13. Phase diagram (composition-structure diagram) of $Na_{2/3}[Mn_{1-x}A_x]O_2$ (A=Co, Li, Ni). The stability regions for P2 and P3 are sketched. M* is mixture of phases.

evaporation and oxygen release. Below the stability region, $Na_{2/3}MO_2$ crystallizes either as P3 or it is a phase mixture.

Fig. 14 shows that the lattice contracts as the cobalt content increases. (The in-plane lattice constant is plotted as either the hexagonal constant a, or $\sqrt{\sqrt{(1/3)}}ab$ for the orthorhombic or monoclinic lattice.) The lattice also becomes less distorted as the Co content increases. Below $x \cong 30\%$ the lattice shows an orthorhombic distortion. Above $x \cong 30\%$ it adopts the ideal P2 structure. Fig. 15 shows the X-ray diffraction pattern and the Rietveld refinement for a distorted ($x=15\%$) and an ideal structure ($x=30\%$). The change from orthorhombic distorted P2 to ideal P2 with increased doping can be understood in terms of the cooperative Jahn–Teller distortion which often occurs if the mean valence state of Mn becomes smaller than $\cong 3.5$. Co prefers the low-spin Co^{3+} state (spherically symmetric) and manganese is either 4^+ or 3^+. For a composition $Na_{2/3}[Mn_{1-x}Co_x]O_2$ the mean manganese oxidation state exceeds 3.5 for $x>1/3$. The transition to the undistorted phase occurs at $x \cong 1/3$ because the symmetric Co^{3+} ions ''dilute'' the effect of the asymmetric Mn^{3+} ions.

The cooperative Jahn–Teller effect decreases the symmetry of the lattice and stretches the MnO_6octahedra, resulting in different Mn–O bond lengths. Unfortunately, the bond lengths cannot be measured from our X-ray data with sufficient accuracy. The strength of the distortion is measured here by comparing the ratio of the b-axis to $3^{1/2}$ times the a-axis. Fig. 16 shows $b/(3^{1/2}a)-1$ plotted versus x in $Na_{2/3}[Mn_{1-x}Co_x]O_2$.

Ion-exchange of the Co doped P2–$Na_{2/3}MnO_2$ is difficult, and never was completed to more than 85% for $x<0.25$. Repeated exchange did not improve the results significantly. The obtained O2–$Li_{2/3}$-$[Mn_{1-x}Co_x]O_2$ has a diffraction pattern which is very similar to the pattern of $Li_{2/3}[Li_xMn_{1-x}]O_2$ which will be discussed later. Electrodes for Li cells were made of $Li_{2/3}[Mn_{0.85}Co_{0.15}]O_2$ and these showed interesting properties. The specific capacity is about 150 mAh/g between 2 and 4.6 V and the material does not convert to spinel upon extended cycling [10]. However, the rate capability is poor.

3.4.2. Lithium doping (the solid solution $Na_{2/3}[Li_xMn_{1-x}]O_2$)

Lithium can replace Mn^{4+} on octahedral sites in Li–Mn spinel and leads to the equilibrium phases $Li[Li_xMn_{2-x}]O_4$ [16]. A similar substitution can be made in the manganese bronzes to make $Na_{2/3}[Li_xMn_{1-x}]O_2$ solid solutions. The maximum substitution limit is reached when the mean manganese oxidation state reaches 4^+, or when $x=2/9$.

A series of samples with $x=0$, 1/18, 0.1, 2/9, 1/6, 2/9 was prepared at temperatures from 700 to 1000°C. Fig. 13 (center plot) shows the stability region for the P2 phase. For $x=1/9$, the P2 phase is stable at $\cong 1000$°C and for $x=2/9$ it is stable near 700°C. The P2 region also has an upper temperature

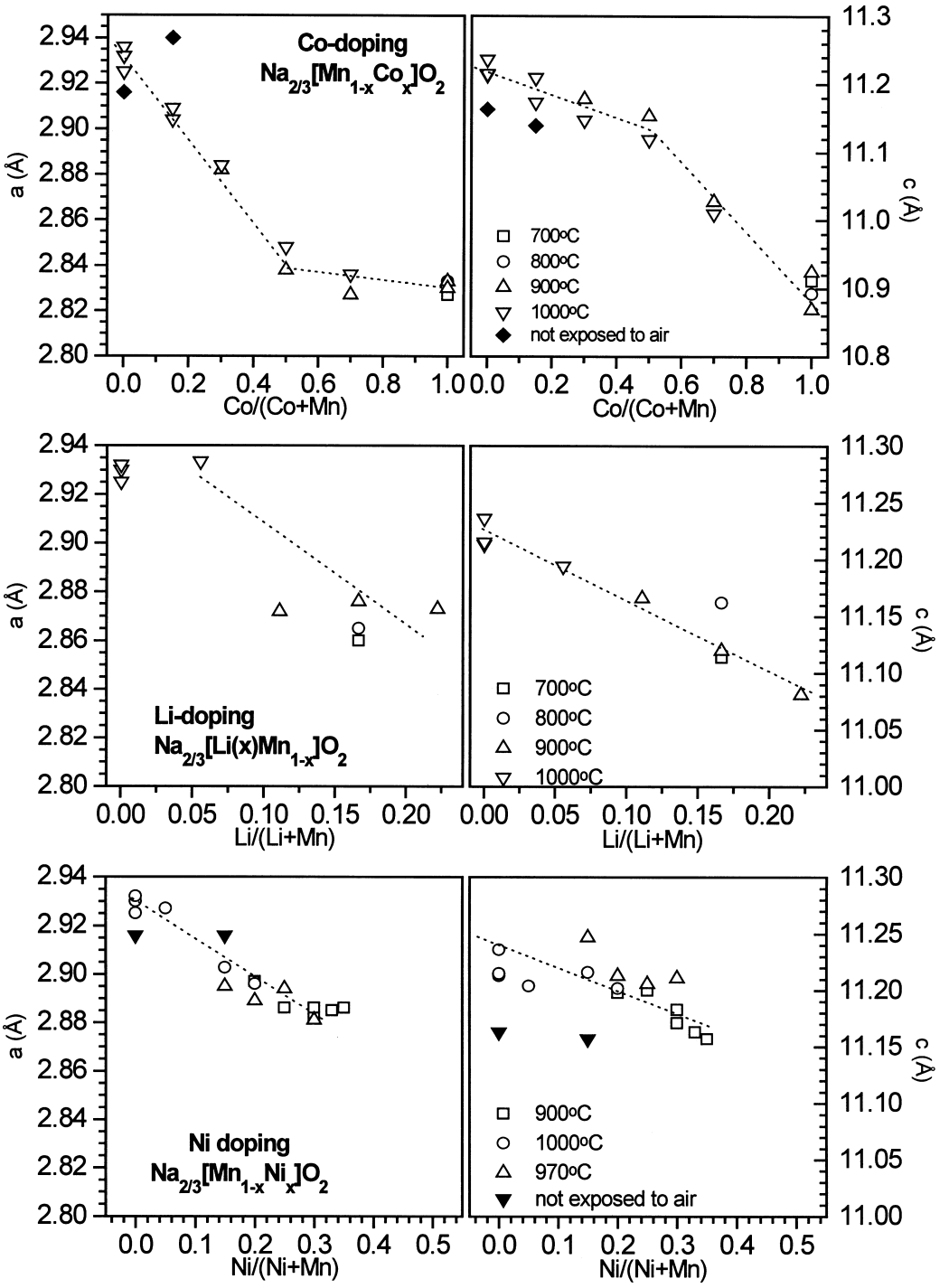

Fig. 14. Hexagonal Lattice constants a and c of P2–$Na_{2/3}[Mn_{1-x}A_x]O_2$ (A = Co, Li, Ni) as a function of *x*. For distorted structures an average hexagonal *a* is calculated from the orthorhombic or monoclinic *a* and *b* (see text).

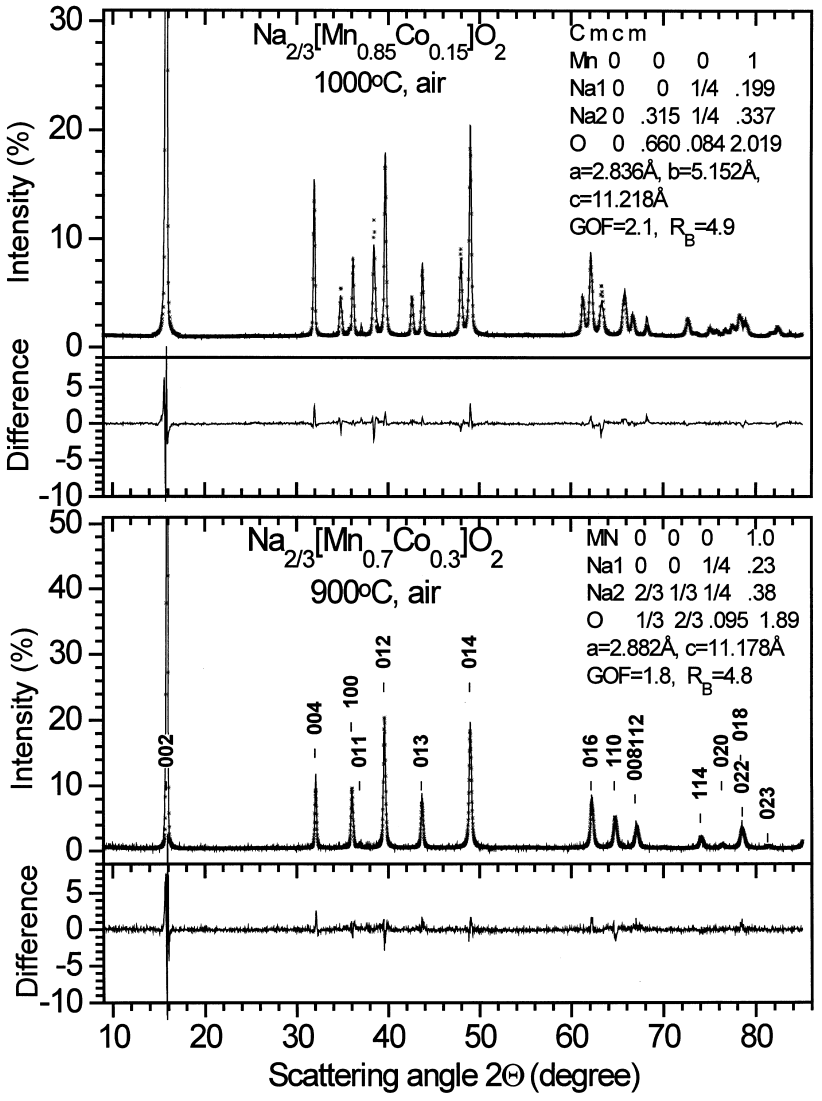

Fig. 15. X-ray diffraction pattern and Rietveld refinement of $Na_{2/3}[Mn_{1-x}Co_x]O_2$. Upper plot: $x=0.15$ (orthorhombic distorted P2). Lower plot: $x=0.30$ (ideal P2).

stability limit that also depends on the lithium concentration. In equilibrium the cationic stoichiometry range at a given temperature is quite narrow.

Lithium is soluble in $Na_{2/3}[Mn_{1-x}Li_x]O_2$ between $x\approx 1/9$ and $x=2/9$. $Na_{2/3}[Mn_{1-x}Li_x]O_2$ with $0<x<1/9$ is a two phase equilibrium of monoclinic distorted P2–$Na_{2/3}MnO_2$ and ideal P2–$Na_{2/3}[Mn_{1-x}Li_x]O_2$ with $x\cong 0.1$. The solid solutions with $x>0.1/9$ exhibit an ideal P2-structure. The mean manganese oxidation state exceeds 3.5 if $x>1/9$, suppressing the cooperative Jahn–Teller distortion. Fig. 17 shows a typical X-ray diffraction pattern for the ideal P2 phase ($x=1/6$).

Ion-exchange in hexanol was almost complete for $x\geq 1/6$ but never for smaller x. The structure of the obtained layered $Li_x[Li_{1/6}Mn_{5/6}]O_2$ is O2 with stacking faults. Layered compounds with stacking faults show sharp peaks for Bragg planes parallel to ($00l$) or perpendicular to the layers ($hk0$), and broad peaks for all other planes. Fig. 17 (lower plot) shows

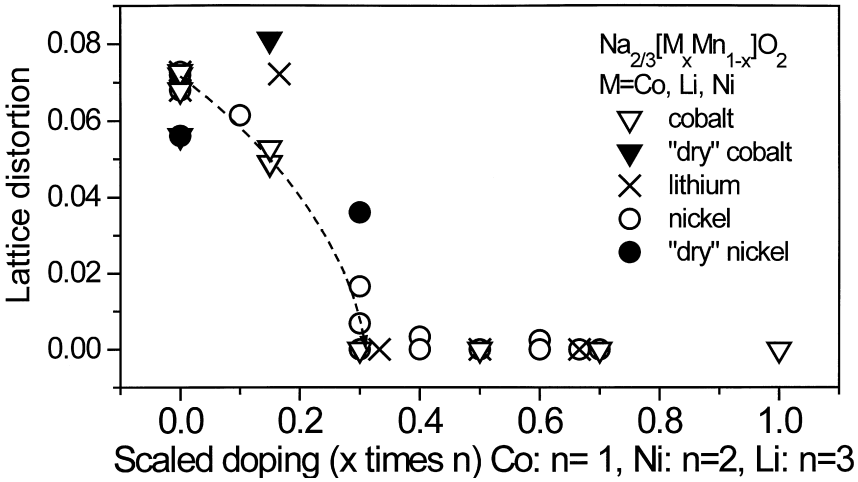

Fig. 16. Lattice distortion as function of scaled doping level as a qualitative measure of the intensity of the Jahn–Teller effect. The *y*-axis is the distortion calculated as $b*3^{-0.5}/a-1$. The scaled doping level is the doping level of Co, Li or Ni multiplied by 1, 3 or 2 respectively. This takes into account that doping by 1 Co/Li/Ni changes 1/3/2 Mn from the trivalent to the tetravalent state.

the diffraction pattern of $Li_x[Li_{1/6}Mn_{5/6}]O_2$. The calculated pattern for O2 (with Miller indices indicated) and O4 phases without stacking faults is also shown. The positions of the sharp 00*l* and *hk*0 peaks coincide with those of experiment, and the strongest broad peaks coincide well with the strongest mixed peaks (e.g. 011, 013 and 015) of the O2 calculation suggesting an O2 or O4 structure with stacking faults. The model is explained in more detail in Ref. [10].

3.4.3. Nickel doping (the solid solution $Na_{2/3}[Mn_{1-x}Ni_x]O_2$)

P2–$Na_{2/3}MnO_2$ can be substituted by up to 33% nickel. The lattice contracts as the Ni content increases (Fig. 14). Fig. 13 shows that Ni substitution extends the stability range of P2 to lower temperatures. $Na_{2/3}[Mn_{1-x}Ni_x]O_2$ ($x=0.05$) is stable at 1000°C but samples with $x=0.33$ can be prepared in pure form at 800°C. Further increase of the Ni content yields phases coexisting with NiO. This limit can be understood if divalent Ni replaces trivalent manganese to make $Na^{I}_{2/3}[Mn^{III}_{1-3x}Mn^{IV}_{2x}Ni^{II}_{x}]O_2$. Then the composition limit is reached at $Na^{I}_{2/3}[Mn^{IV}_{2/3}Ni^{II}_{1/3}]O_2$.

Since nickel is divalent the mean Mn oxidation state will exceed 3.5 and suppress the Jahn–Teller distortion if x becomes larger then 1/6. Indeed, when $x=0.05$ an orthorhombic distorted P2-structure is found, but a sample with $x=0.15$ shows a P2-structure which is weakly distorted. If exposed for a longer time to air this distortion disappears and the structure approaches the ideal P2. For $0.15<x\leq 0.33$ the structure is undistorted. Fig. 18 shows the typical X-ray patterns for the orthorhombic ($x=0.05$) and ideal structure ($x=0.30$) together with the Rietveld refinement. The decrease of the Jahn–Teller distortion with doping is shown in Fig. 16.

Ion-exchange of $Na_{2/3}[Mn_{1-x}Ni_x]O_2$ in molten salt was complete and yielded crystalline $Li_{2/3}MO_2$ if x was near 0.33. To our knowledge this is the first report of a crystalline O2–Li–Mn oxide. The X-ray diffraction results for a sample of $Li_{2/3}[Ni_{1/3}Mn_{2/3}]O_2$ are given in Fig. 19. The spectrum is very similar to that of the ideal O2-structure ($P6_3mc$), however, the (superstructure ?) peaks at 66° (111) and 72°C (113) are forbidden in the ideal O2 structure and the peak at 79.5° (202) is much too intense. These peaks would be allowed using a superstructure (3 times larger unitcell) in the space group P31m. However, we did not achieve a satisfactory refinement yet. Understanding this pattern fully will be the subject of further work.

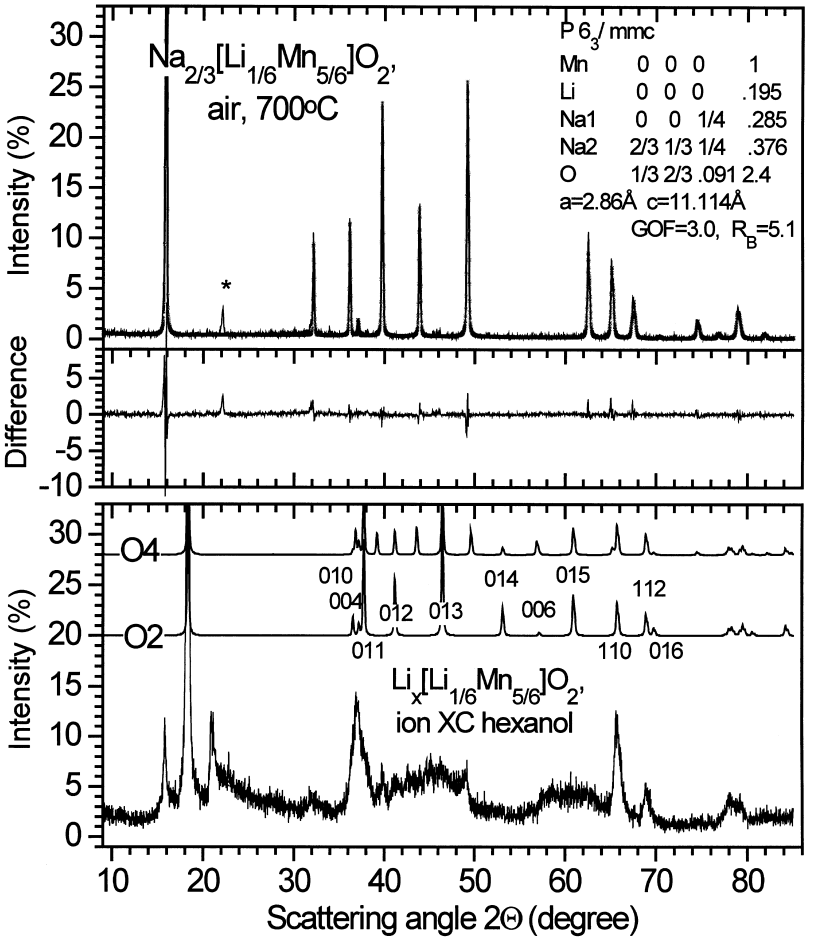

Fig. 17. Lithium doped P2–$Na_{2/3}MnO_2$ and the ion-exchanged derivatives of $Na_{2/3}[Li_xMn_{1-x}]O_2$. Upper plot: $Na_{2/3}[Li_{1/6}Mn_{5/6}]O_2$, $x=1/6$ (ideal P2). Lower plot: O2-type $Li_x[Li_{1/6}Mn_{5/6}]O_2$ obtained by ion-exchange.

3.5. Thermal and chemical stability

Water plays an important role in P2-structure manganese bronzes. We observed that weakly substituted or unsubstituted samples are hygroscopic. To investigate this, samples of $Na_{2/3}MO_2$ (M=Mn, M=$Mn_{0.85}Co_{0.15}$ and M=$Mn_{0.85}Ni_{0.15}$) were investigated without exposure to air. Fig. 20 shows the diffraction patterns obtained. The changes compared with samples exposed to air are not dramatic. Exposed $Na_{2/3}MnO_2$ (Fig. 7) has a monoclinic distortion whereas the ''dry'' sample has an orthorhombic distortion. The exposed $Na_{2/3}[Mn_{0.85}Co_{0.15}]O_2$ (Fig. 15, upper plot) and the ''dry'' sample have an orthorhombic distortion which is more pronounced in the ''dry'' case. The same trend is observed for Ni: The ''dry'' $Na_{2/3}[Mn_{0.85}Ni_{0.15}]O_2$ has a distortion comparable in magnitude to exposed $Na_{2/3}[Mn_{0.85}Co_{0.15}]O_2$ which vanishes for exposed $Na_{2/3}[Mn_{0.85}Ni_{0.15}]O_2$. The change of the diffraction pattern (and of the mechanical properties; after air exposure the material seems to be softer and more layered) clearly indicate a water uptake. However the lattice spacing remains almost constant. This contradicts a ''normal'' intercalation of water molecules between the layers that

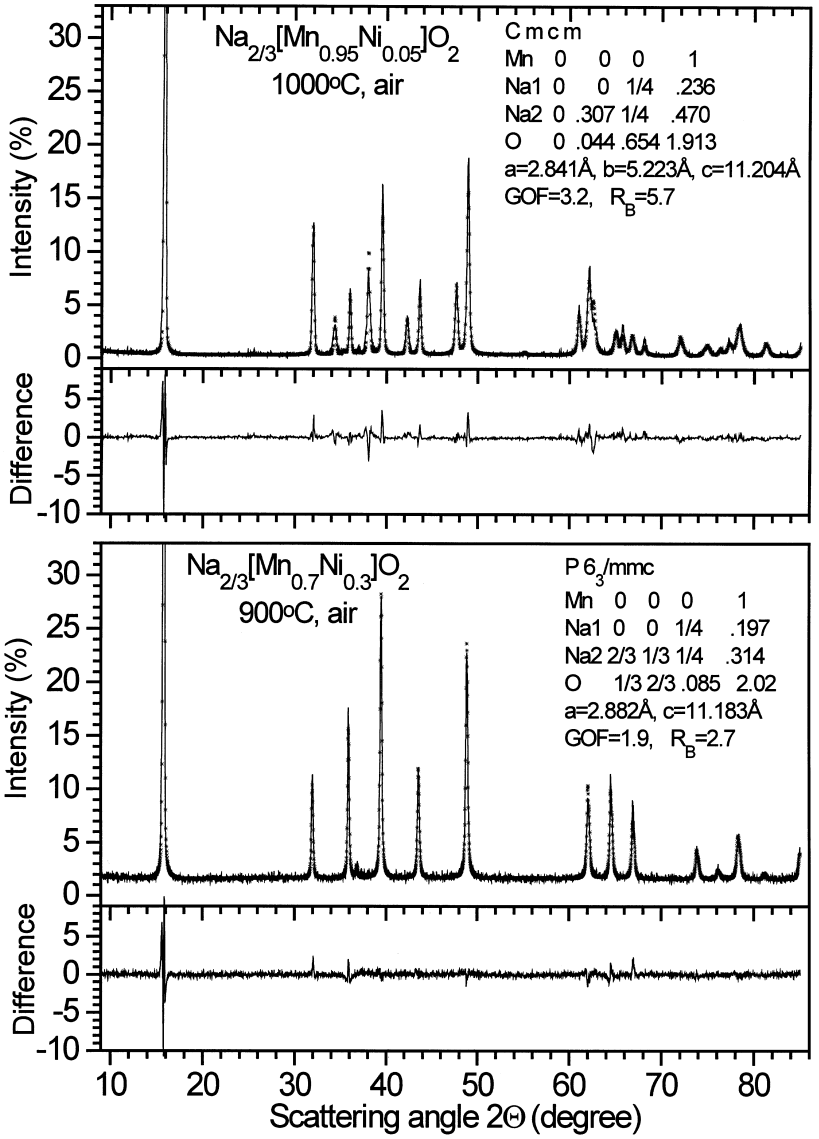

Fig. 18. X-ray diffraction pattern and Rietveld refinement of $Na_{2/3}[Mn_{1-x}Ni_x]O_2$. Upper plot: $x=0.05$ (orthorhombic distorted P2). Lower plot: $x=0.30$ (ideal P2).

would lead to large changes of the layer spacing. Possibly, the oxygen of the water molecules fill oxygen vacancies. Simultaneously, the protons could fill places near to empty sodium sites.

The samples are air stable but severe water exposure can damage them. Weakly substituted samples do not tolerate boiling in water. After some hours they totally decompose to materials with a large *c* spacing. Such spacing is typical for minerals that contain significant amounts of water between the manganese oxide sheets. Heavily substituted samples are more stable with respect to water: Their X-ray spectrum did not change after exposure to air, the mechanical properties were unaffected, and boiling in water caused less severe damage.

In this work the majority of the ion-exchange was

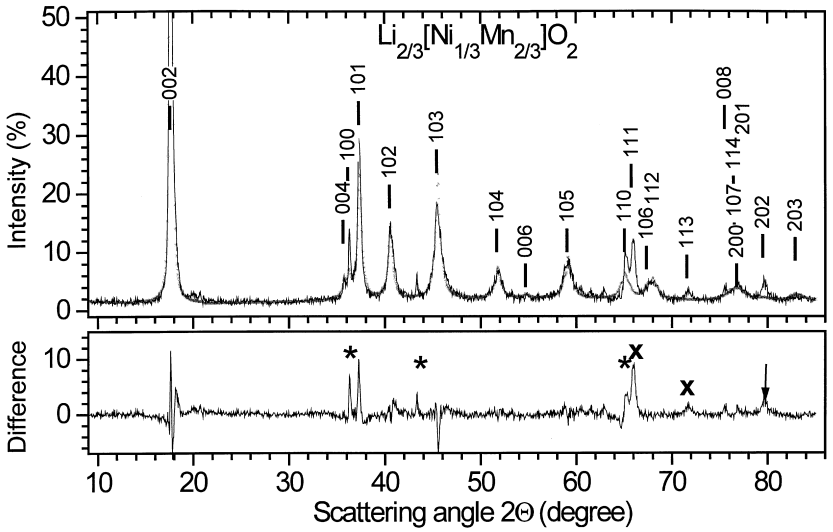

Fig. 19. X-ray diffraction pattern and Rietveld refinement of O2–$Li_{2/3}[Ni_{1/3}Mn_{2/3}]O_2$. The asterisk marks impurity peaks due to spinel or $[Li_{1-x}Ni_x]NiO_2$, the × marks (superstructure ?) peaks which are forbidden in the ideal O2-structure.

made using hexanol. Any alcohol is slightly reducing. Therefore, a reduction or an ion-exchange of the sodium by protons instead of lithium could be possible. To check this a sample $Na_{2/3}[Mn_{0.85}Co_{0.15}]O_2$ was heated for 3 days in hexanol at 150°C. The X-ray diffraction pattern changed only slightly. Peak positions were unchanged. However, the peaks became slightly broader, and the intensity of superstructure peaks due to the orthorhombic distortion became weaker. A tiny peak emerged at 18°, a typical position for the average peak of ion-exchanged phases. However, it can be concluded that the samples are stable at least during the time of the ion-exchange reaction.

The layered lithium transition metal oxides with the O2-structure are surprisingly stable. DSC investigation does not show a transition O2→O3. This could be due to slow kinetics or small heat of reaction. X-ray diffraction shows that O2–$LiCoO_2$ starts to transform to O3–$LiCoO_2$ after some hours at 230°C. At 400°C approximately 60% of the O2 phase is transformed after 1 h. However, after 8 h some small amount of O2–$LiCoO_2$ remains. O2–$Li_{2/3}[Mn_{2/3}Ni_{1/3}]O_2$ is much more stable. At 400°C, 4 days were needed to evolve minor contributions of the thermodynamically stable $Li_4Mn_5O_{12}$ type spinel and $[Li_{1-x}Ni_x]NiO_2$; whereas after 1 day at 400°C no decomposition was detectable by X-ray diffraction.

4. Summary

P2-sodium manganese bronzes were investigated. The properties can be modified by doping with Li, Co or Ni. If the doping level is increased the Jahn–Teller distortion becomes suppressed and the crystal structure becomes more ''ideal P2''. Doping extends the stability region of P2 towards lower temperatures. To design special structures thermal treatments as ''thermal shock'' and ''soft oxidation'' are suggested. The P2 phases were used to prepare metastable Li–Mn oxides, which exhibit the O2 structure. Often the O2-structure materials exhibit poor crystallinity caused by stacking faults. However, the ''stoichiometric'' phases O2–$LiCoO_2$ and O2–$Li_{2/3}[Ni_{1/3}Mn_{2/3}]O_2$ are well ordered. The latter is the first report of a crystalline O2-type phase based on Li–Mn-oxide.

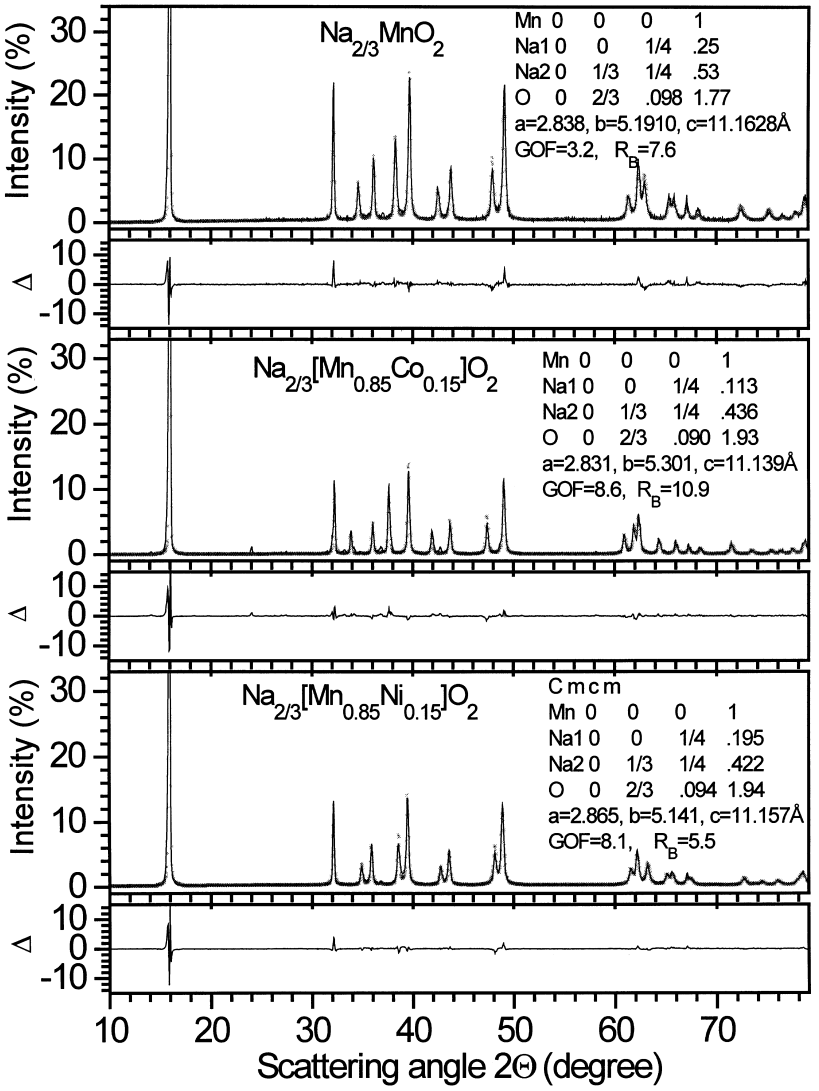

Fig. 20. X-ray diffraction patterns of $Li_{2/3}[M]O_2$ without air exposure. Upper plot: M = Mn, Middle plot: $M = Mn_{0.85}Ni_{0.15}$, Lower plot: $M = Mn_{0.85}Ni_{0.15}$.

References

[1] C. Delmas, J.-J. Braconnier, A. Maazaz, P. Hagenmuller, Revue de Chimie Minerale 19 (1982) 343.

[2] F. Capitaine, P. Gravereau, C. Delmas, Solid State Ionics 89 (1996) 197.

[3] A.R. Armstrong, P.G. Bruce, Nature 381 (1996) 499.

[4] C. Delmas, J.-J. Braconnier, P. Hagenmuller, Mat. Res. Bull. 17 (1982) 117.

[5] J.-P. Parant, R. Olazcuaga, M. Devalette, C. Fouassier, P. Hagenmuller, J. Solid State Chem. 3 (1971) 1.

[6] C. Delmas, C. Fouassier, P. Hagenmueller, Physica 99B (1980) 81.

[7] C. Delmas, J.-J. Braconnier, C. Fouassier, P. Hagenmuller, Solid State Ionics 3/4 (1981) 165.

[8] A. Mendiboure, C. Delmas, P. Hagenmuller, J. Solid State Chem. 57 (1985) 323.

[9] L.W. Shacklette, T.R. Jow, L. Townsend, J. Electrochem. Soc. 135 (1988) 2669.

[10] J.M. Paulsen, C.L. Thomas, J.R. Dahn, accepted for publication in J. Electrochem. Soc. (1999).

[11] L.V. Gurvich, V.S. Iorish, D.V. Database on Thermodynamic Properties of individual substances, vers. 1.01, Russian

Academy of Science, version 1.01, ©Begell House Inc., 1993.
[12] R.J. Hill, C.J. Howard, J. Appl. Crystallogr. 18 (1985) 173.
[13] D.B. Wiles, R.A. Yong, J. Appl. Crystallogr. 14 (1981) 149.
[14] Landolt-Börnstein, II. Band, 3. Teil ''Schmelzgleichgewichte und Grenzflächenerscheinungen'', Springer Verlag Berlin, Göttingen, Heidelberg, 1956, pp. 138.
[15] C. Fouassier, G. Matejka, J.-M. Reau, P. Hagenmueller, J. Solid State Chem. 6 (1973) 532.
[16] J.M. Paulsen, J.R. Dahn, Chemistry of Materials, accepted for publication.